PREDICTION OF THE EFFECT OF NONLINEAR PROPAGATION DISTORTION IN BLADE VORTEX INTERACTION NOISE

Penelope Menounou and **Panagiotis Vitsas**

Department of Mechanical and Aeronautical Engineering

University of Patras, Patras, Greece

Nonlinear propagation distortion causes energy to be shifted to the high-frequency-end of the spectrum. As a result, traditional linear calculations, that include geometrical spreading and atmospheric absorption, underestimate the noise levels at high frequencies. The effect has been investigated for aircraft jet noise, but less attention has been given to helicopters. The Burgers equation, which incorporates nonlinear propagation distortion effects, is employed for the prediction of the noise spectrum away from the helicopter. It is shown that nonlinear effects can be sizeable for Blade Vortex Interaction noise produced by helicopter's main rotor. However, employment of the Burgers equation can be time consuming to be included in routine calculations. It also requires knowledge of the initial pressure time signal. The power spectrum alone, which is usually known, is not sufficient. In the present work, three predictions methods are presented that are based on the Burgers equation and address the above concerns.

1 Introduction

All parts of a noise signal with relatively low amplitude (small signal or linear case) propagate with the same velocity, namely the speed of sound. As a result, all points of the signal maintain their position with one-another and the shape of the signal remains the same throughout the propagation. In the finite-amplitude or nonlinear case, (in other words, when the noise signal is of high intensity), each part of the signal travels with its own velocity, namely the speed of sound plus the local velocity of the signal. Parts of the signal travel faster than the speed of sound, while others move slower. As a result, the original shape of the signal distorts and its frequency distribution changes accordingly. The effect has been studied in aircraft jet noise propagation, where it has been demonstrated that ignoring nonlinear effects can lead to underestimation of the high frequency end of the spectrum [1,2,3]. Little, however, has been done on helicopter noise propagation [4]. In the present work, we demonstrate the effect of nonlinear propagation distortion in helicopter rotor noise and we present three ways, based on the Burgers Equation, for the evaluation of the effect for Blade Vortex Interaction (BVI) noise.

2 Numerical Prediction by Burgers Equation

For the prediction of nonlinear propagation distortion the augmented Burgers Equation (BE) is employed [5,6]:

$$\frac{\partial P}{\partial r} = -\frac{1}{r}P + \frac{\beta}{\rho_o c_o^3} P\frac{\partial P}{\partial \tau} + \frac{\delta}{2c_o^3}\frac{\partial^2 P}{\partial \tau^2} + \sum_\nu \frac{c_\nu'}{c_o^2}\int_{-\infty}^{\tau} \frac{\partial^2 P}{\partial \tau'^2} e^{-(\tau-\tau')/t_\nu} d\tau' , \quad (1)$$

where P is the sound pressure, r the propagation distance, $\tau = t-(r-r_0)/c_0$ the retarded time with r_0 being the radius of the spherical sound source, ρ_0 is the ambient density, c_0 the small signal sound speed, β the coefficient of nonlinearity, δ the diffusivity of sound for viscosity and heat conduction, $\nu = 1,2$ is the index of the two relaxation processes (of O_2 and N_2), each characterized by a relaxation time t_ν and the corresponding net increase c_ν' in phase speed as frequency varies from zero to infinity. The first term in the right hand side of Eq. (1) describes the spherical spreading, the second the nonlinear distortion, the third the thermoviscous attenuation, while the forth describes the attenuation due to relaxation effects of O_2 and N_2 in real atmosphere. Giving an initial pressure time signal, the BE predicts the evolution of the time signal as it propagated through the atmosphere. The BE is solved numerically by the algorithm of Cleveland-Hamilton-Blackstock.[7,8] In the following, *linear predictions* shall mean solution of the BE without including the nonlinear term in Eq. (1), while *nonlinear predictions* shall mean solution of the BE including the nonlinear term.

Predictions using the BE on helicopter noise signals show that nonlinear effects can be important in some cases. Figure 1 shows comparisons between experiments and predictions employing Eq. (1) with and without the nonlinear term. It can be observed that nonlinear propagation distortion effects explain the differences between measurements and linear predictions. The experimental data are from Ref. 9 and regard high speed impulsive noise. Measurements were taken at two microphones positioned in the rotor plane along a line from the rotor hub directly ahead of the rotor, the first microphone at twice the distance of the second, 3.4 and 1.7 rotor diameters, respectively. The ratio of the peaks of the two pressure signals was reported as a function of advancing tip Mach number. The ratio deviated from the expected value of 2 for high advancing tip Mach numbers, particularly above the delocalization Mach number

($M_{AT} \simeq 0.90$). The comparison illustrated in Figure 1 shows the prediction capability of the BE, as well as, the importance of nonlinear effects in helicopter noise.

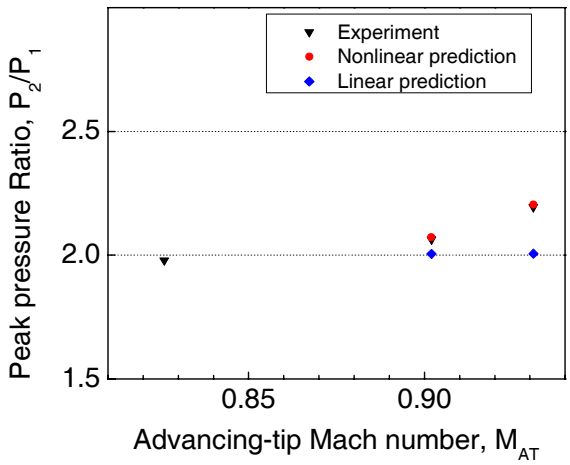

Figure 1: Nonlinear propagation distortion can explain differences between measurements and linear predictions; experimental data from Ref. 9 for high speed impulsive noise; numerical predictions employing Eq. (1)

Figure 2 shows the difference between linear and nonlinear predictions for low speed descend, when BVI noise is dominant. The receiver is 500m below the rotor disc, in front of the helicopter and on the 47 degrees longitudinal angle propagation line. The source signals are taken from HELISHAPE experimental data [10]. Unlike the previous case of high speed impulsive noise, where the noise signals contained shocks and had large pressure amplitudes (800 Pa), the BVI noise during low speed decent is of smaller amplitude (70 Pa) and is shock free. It can be observed, however, that nonlinear propagation distortion affects the spectrum even in this case. The frequencies affected are 1000Hz - 3000 Hz.

Spherical spreading is the mechanism that mainly determines the evolution of the noise spectrum. Atmospheric absorption, although less important, is routinely included in the calculations. Figure 3 shows that nonlinear propagation distortion affects the evolution of the spectrum at much as the atmospheric absorption. It should, therefore, be included in the computations to increase the accuracy of predictions.

The employment BE for the numerical prediction has two main difficulties: (i) it can be time consuming to be included in routine calculations, as for example, in optimization of noise abatement procedures; and (ii) it requires knowledge of the initial pressure time signal, the power spectrum alone, which is usually known, is not sufficient. In the following three approaches are presented to address these concerns.

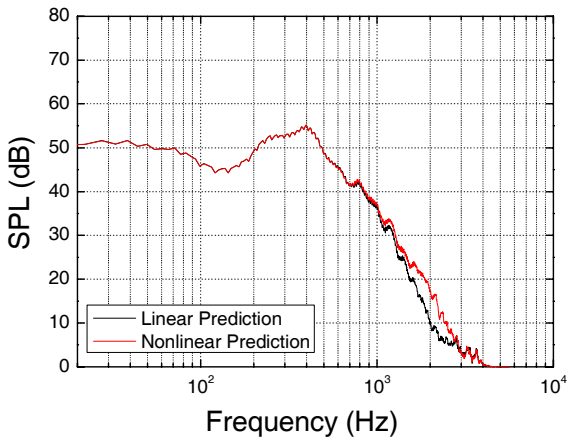

Figure 2: Comparison between linear and nonlinear predictions of the BVI noise spectrum after 500m of propagation; numerical predictions from Eq. (1); noise source signals from HELISHAPE measurements [10] for low speed decent;

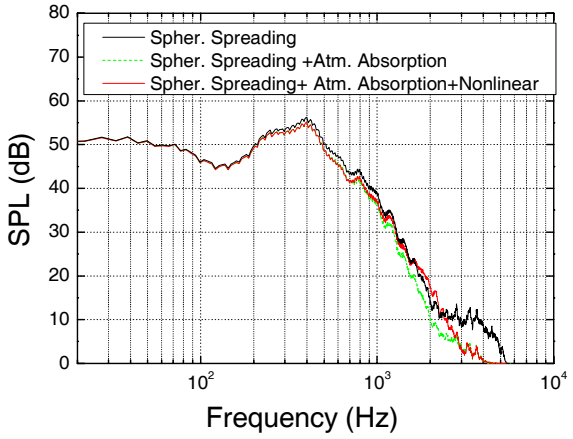

Figure 3: Comparison of the magnitude of the effects of: (i) geometrical spreading, (ii) atmospheric absorption, and (iii) nonlinear propagation distortion in the case of the noise spectrum in Figure 2.

3 Numerically Generated Database

To address the concern regarding the complexity of the nonlinear calculations, a numerically generated database has been created specifically for BVI noise. Measurements (pressure time histories) from the HELISHAPE experiment for low speed descent [10] have been used as noise source signals and their nonlinear evolution has been stored in the database.

HELISHAPE measurements were done in the DNW wind tunnel with a four bladed model rotor having a rectangular blade tip shape. The flight speed was 35 m/s, and the descent flight had a -6 deg path angle. Measurements were made at an array of 11 equally spaced microphones (see Figure 4) with the array's span positioned normal to the flow, symmetrically arranged with respect to the rotor center, and at several streamwise locations of the array's span. [10]

The noise signals measured on the microphone grid were considered as noise source signals coming from a

directive stationary point source located at the rotor center and with source radius equal to the distance from the rotor center to the given microphone position. The noise signals were first transformed into full scale data [11], and were subsequently propagated numerically distance R following the propagation path from the rotor head center through the microphone grid to receiver locations on the surface of a hemisphere as shown in Figure 4. The calculations have been performed employing Eq. (1) twice, once including only linear propagation effects (geometrical spreading and atmospheric absorption) and a second time adding nonlinear propagation distortion to the linear calculations. In the following, the microphone number and the streamwise position of the microphone array (for example Mic 6/ x=0) will indicate the set of measurements performed using as noise source signal the signal measured at the position identified by its streamwise position and microphone number.

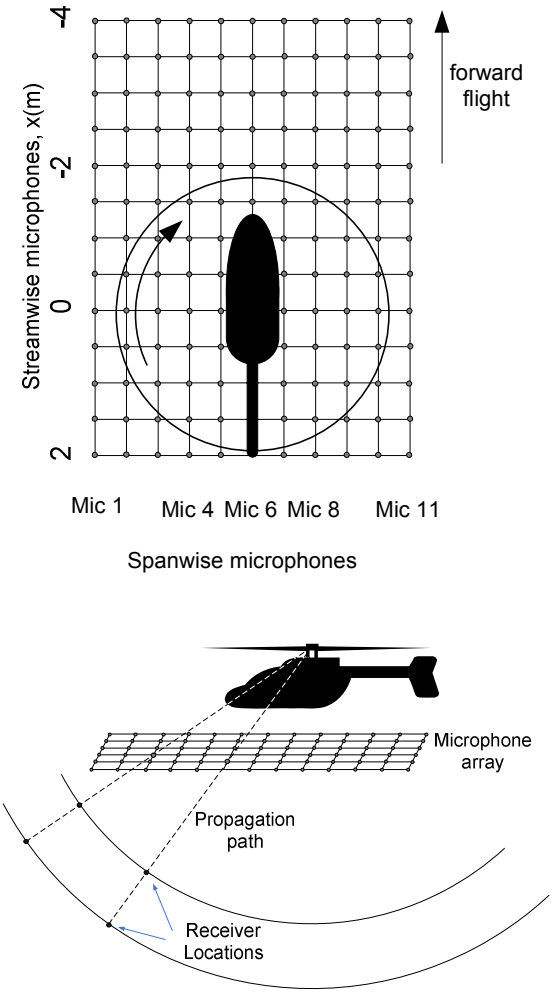

Figure 4: Measurements positions in HELISHAPE experiment (above); propagation path in the numerical calculations (below).

The database provides the difference in the SPL value with and without the nonlinear effects after propagation distance R as a function of frequency f:

$$DSPL = SPL_{nonlinear}(f;R) - SPL_{linear}(f;R). \qquad (2)$$

Data are provided at 143 points on a hemisphere and for 18 different hemisphere radii ranging from 20m to 1.5km - a total of 143X18=2574 receiver locations. The numerically generated database has been integrated into HELENA, a computational tool synthesized under the integrated European project FRIENDCOPTER. When only the receiver location is known, the database serves as a rough guideline that provides the correction to SPL values obtained with traditional linear calculations so that nonlinear effects are accounted for.

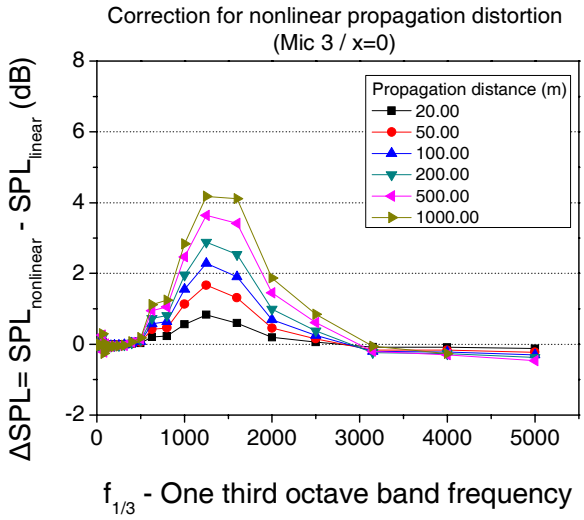

Figure 5: Example result from the numerically generated database; DSPL at one-third octave frequency bands for various propagation distances; predictions based on noise source signals measured at Mic 3 / x=0 (Figure 4).

Figure 5 shows an example result from the numerically generated database. It has been shown [12] that the nonlinear evolution of all measured BVI signals is either of the advancing side type (as the one shown in Figure 5) or of the retreating side type. In the following we will be focus our attention in the prediction of the advancing side type nonlinear evolution, because this concerns the majority of the receiver locations and because the retreating side type yields negligible DSPL values. It can be observed that (i) DSPL values are predominantly positive (in other words linear calculations under-predict the noise spectrum), (ii) the octave frequency bands affected are the bands centered at 1000 Hz and 2000 Hz, to which the human ear is most sensitive, and (iii) that the DPSL values increase with increasing propagation distance, until the SPL values diminish themselves with propagation distance, mainly by spherical spreading, and cannot longer be heard.

The overall A-weighted SPL value (OASPL) does not increase appreciably by nonlinear effects. This is attributed to the fact that OSPL is mostly determined by the largest SPL values of the spectrum. For helicopters, this is the low frequency end of the spectrum, which, however, remains unaffected by nonlinear effects.

Finally, an important observation is the strong dependence of DSPL on the receiver location, as demonstrated in Figure 6. Figure 6 shows the DSPL predicted on a plane 120 m below the main rotor for the

one-third-octave frequency bands centred at 1250Hz, 1600Hz, 2000Hz, and 2500Hz for both advancing and retreating side BVI regions. It can be observed that the one-third-octave frequency bands of 1600 Hz and 2000 Hz are mostly affected. It should also be noted that the effect is not spatially uniform but depends strongly on the receiver locations.

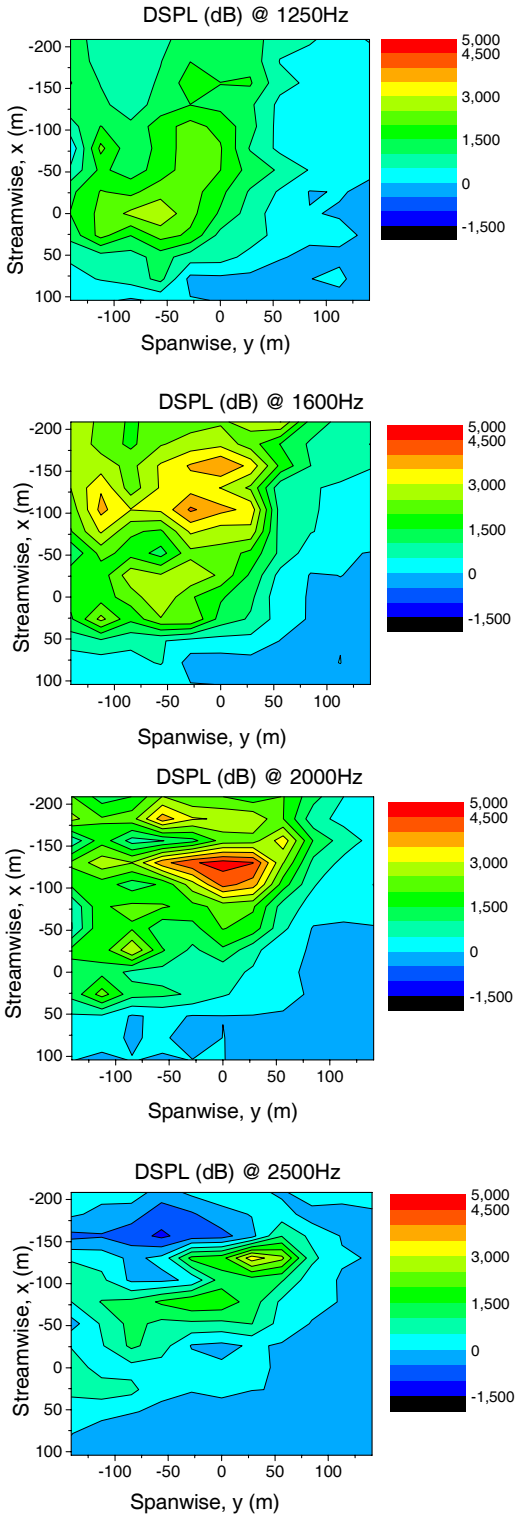

Figure 6: DSPL depends strongly on the receiver location; DSPL shown on a plane 120m below the rotor head center; DSPL shown at one-third-octave frequency bands centred at 1250Hz, 1600Hz, 2000Hz, and 2500Hz.

4 Correlations

In the present section a second remedy is presented that addresses the concern regarding the complexity of the nonlinear calculations. Correlations between predicted DSPL values after propagation and characteristics of the source signal have been investigated. The correlations established from the analysis of the database in hand can be used to provide an estimated of DSPL in the propagation of other BVI noise signals. This will, in turn, determine if a detailed prediction of nonlinear effects employing the BE is merited.

Further, it should be mentioned that data points corresponding to retreating side type nonlinear evolution have been excluded from the correlations. The correlations regard, therefore, advancing side type nonlinear evolution. As mentioned earlier, this type characterizes the majority of receiver locations and provides sizeable DSPL values, as opposed to the retreating side type, which yields negligible DSPL.

4.1 Predictors and Nonlinear Quantities

Many characteristics of the source signals have been investigated. More specifically, the following signal characteristics, as well as many of their combinations haven been considered: $OSPL$, $P_{\max}$, $(dP/dt)_{\max}$, kyrtosis, skewness, CF (crest factor), $DP_{\max}$ (maximum pressure difference between neighbouring points in the digitized time signal), LF (SPL comprising low frequency levels from the 2nd to the 10th blade passage frequency harmonics (bpfh); an approximate measure for thickness and high speed noise), MF (SPL comprising mid frequency levels from the 6th to the 40th bpfh; an approximate measure for BVI impulsive noise), and HF (SPL comprising frequency levels from the 40th to the 156th bpfh; an approximate measure that was found to describe the effect of nonlinearity).

The above signal characteristics have been correlated with the following quantities that describe nonlinear distortion: $DSPL$ at the 1/3 octave frequency bands centred at 1600 Hz, 2000Hz and 2500 Hz, $DSPL_{\max}$ -the maximum value of $DSPL$ irrespective of the one-third octave frequency band at which it occurs, and $DSPL$ at the octave frequency bands centred at 1000Hz and 2000Hz. The correlations of the above nonlinear quantities with the source signal characteristics have been performed at propagation distances of 120m, 300m, 500m and 1000m.

Only five of the many predictors investigated provided a good correlation with the nonlinear quantities. Specifically, $P_{\max} X\ CF$, $DP_{\max}$, $(dP/dt)_{\max}$, $P_{\max} X\ skewness$, and HF. Some of the remaining predictors did not correlate well with the nonlinear distortion quantities, while others failed in predicting the area below the helicopter affected by nonlinear effects. Consider, for example, the predictor $OSPL$, that characterizes the intensity of the noise source signal. It could, thus, provide an indication on nonlinear effects. However, by observing Figure 7 it can be concluded that

areas of high value of *OSPL* do not coincide with areas of high value of DSPL as illustrated in Figure 6.

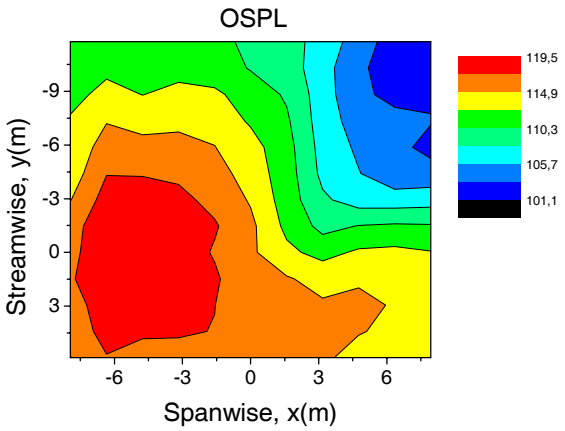

Figure 7: OSPL of the noise source signals at a plane below the rotor head center (measurement positions).

4.2 Correlations between Predictors and Nonlinear Quantities

Figure 8 shows examples of correlations between $DSPL_{\max}$ and the five predictors: $P_{\max} X\ CF$, $DP_{\max}$, $(dP/dt)_{\max}$, $P_{\max} X\ skewness$, and HF after 120 m of propagation distance.

The good correlation can be observed. Lines are fitted between the points in the graphs. The equations of the fitted lines are to be used for predicting $DSPL_{\max}$ after 120 m of propagation distance:

$$DSPL_{\max} = -0.08315 + 0.01509\left(P_{\max} X\ CF\right) \quad (3)$$

$$DSPL_{\max} = -0.3661 + 0.2946 DP_{\max} \quad (4)$$

$$DSPL_{\max} = 12.95 - 0.4273 HF + 0.003464 HF^2 \quad (5)$$

$$DSPL_{\max} = 0.9003 + 0.03519\left(P_{\max} X\ skewness\right) \quad (6)$$

$$DSPL_{\max} = 0.1810 + 0.000027\left(\frac{DP}{Dt}\right)_{\max} \quad (7)$$

Similar equations can be derived for the other nonlinear quantities and for all propagation distances.

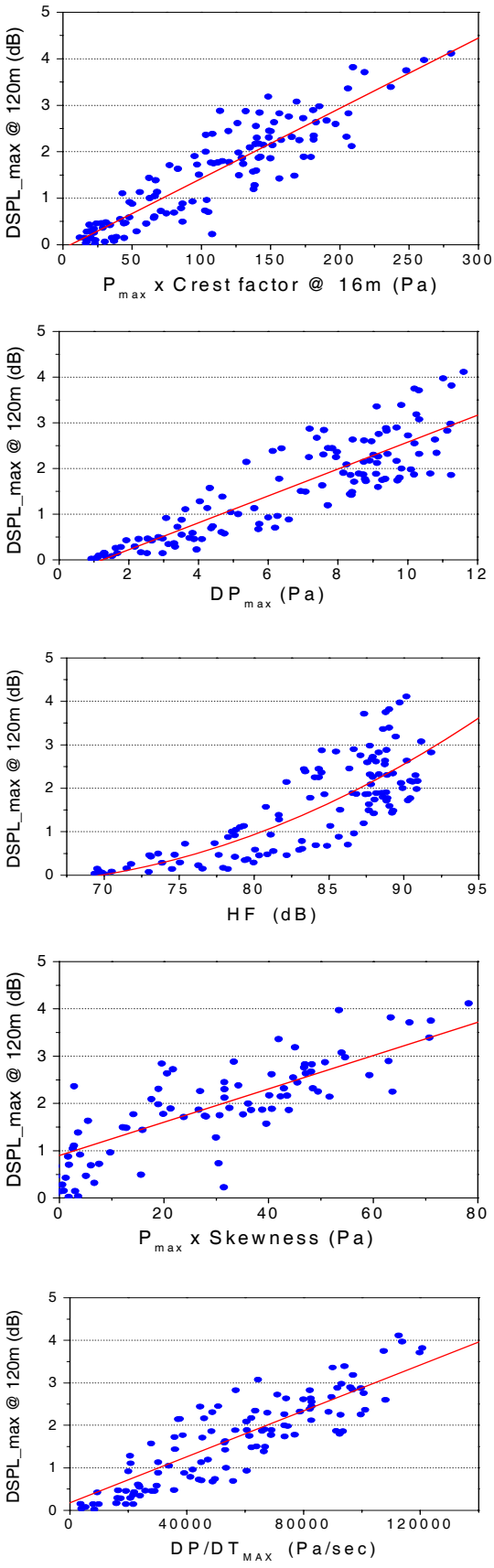

Figure 8: Correlations between $DSPL_{\max}$ after 120m of propagation and characteristics of the noise source signals (predictors).

4.3 Prediction Examples

The correlations presented in the previous subsection are used to make predictions, which are subsequently checked against a second numerically generated database. The second database is generated similarly to the first one and is based on a different set of HELISHAPE measurements. The flight conditions and the measuring points were the same, but the rotor with a swept-back parabolic-anhedral tip was used instead of the rectangular blade tip. Because the noise source signals are different at the two databases, their nonlinear evolution is also different. The correlations, however, can be used to provide only an estimate of DSPL.

Table 1 shows an example of the $DSPL_{\max}$ calculation for Mic 3 / x=-1 after 120 m of propagation. The source data at Mic 3 / x=-1 are analyzed first and the value of the five predictors ($P_{\max} X\ CF$, $DP_{\max}$, $(dP/dt)_{\max}$, $P_{\max} X\ skewness$ and HF) are computed. Based on the values of the five predictors and Eqs (3) -- (7) estimates of $DSPL_{\max}$ are computed, numerically averaged and compared against the $DSPL_{\max}$ in the second database for point Mic 3/ x=-1 after 120 m of propagation. The predicted value is very close to the real one.

Figure 9 shows the difference between the predicted values $DSPL_{\max}$ (based on the correlations and computed as described above) and the real values of $DSPL_{\max}$ after 120m of propagation for several noise source signals. It can be observed that the predictions agree reasonably well with the real DSPL values. The derived correlations, therefore, can be used to provide an estimate of the effect of nonlinear propagation distortion based on the noise signal characteristics at source for similar helicopter rotors.

Table 1: $DSPL_{\max}$ after 120m of propagation for the noise source signal measured at Mic 3/ x=-1; predictions using characteristics of the noise source signals and Eqs (3) - (7); comparison with $DSPL_{\max}$ yielded by employing Eq. (1) for the propagation of the same noise source signal; noise source signal from the second database

Noise prediction	Mic 3 / x=-1	
Predictors	source_data	$DSPL_{max}$ (dB)
P_{max} x CF	196,13	2,8764517
DP_{max}	11,999	3,1688054
HF	90,09	2,569087858
P_{max} x skewness	39,162	2,27841078
$(dP/dt)_{max}$	50215,349	1,536814423
average predicted $DSPL_{max}$ (dB)=		2,485914032
actual $DSPL_{max}$ (dB)=		2,36
deviation (dB)=		0,125914032

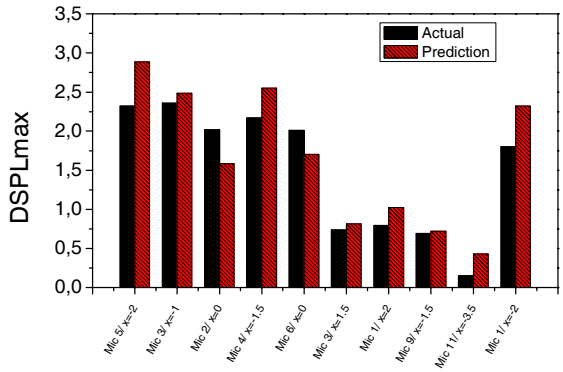

Figure 9: Comparison between $DSPL_{\max}$ after 120m of propagation predicted from Eqs (3) - (7) (solid) and by employing Eq. (1) (pattern); noise source signals from the second database; noise source signals measured at the locations indicated in the horizontal database.

5 Phase Assignment

The problem of the missing phase information is addressed next. Often the power spectrum of helicopter noise is provided, not the signal itself. A given pressure time signal corresponds to a unique power spectrum. On the contrary, to a given power spectrum corresponds an infinite number of pressure time signals, each having a different phase distribution. The phase distribution affects the shape of the signal and in turn its nonlinear distortion. In the cases of aircraft noise, a random phase uniformly distributed in $[-\pi : \pi]$ is assigned in order to re-construct the pressure time signal. This method is inappropriate for helicopter noise, as it eliminates the characteristic pulses contained in a helicopter noise signal. The present work proposes the assignment of constant phases, in addition to random phases, in appropriately selected frequencies. The aim of the proposed phase assignment is to create a signal whose main BVI pulse will be similar enough to the main BVI pulse of the real signal time signal so that both the re-constructed and the real time signal exhibit the same nonlinear behavior.

5.1 Frequency Regions

For the application of the phase assignment method the spectrum of the noise source signals is divided into three regions.

a) Thickness region

The region from the 2nd to the 10th blade passage frequency harmonic (bpfh) [10], or alternatively from the 2nd to the 5th bpfh [13], is considered to be an approximate measure for thickness and high speed noise. In the signals of our database thickness noise was found to be most evident in the region from the 1st up to the 5th bpfh.

b) Main BVI pulse region

The BVI frequency region is defined as the region from the 6th to the 40th bpfh [14], or from the 5th to the 30th [15]. In the signals at hand the start of the BVI region occurs at

the 5th bpfh, while the ending frequency varies with the microphone position, from the 50th bpfh for the less impulsive signals to the 80th bpfh for the more impulsive. As this region is by definition discrete, the end of the region is determined by visual observation (see Figure 10).

c) Broadband region

For the signals at hand broadband noise includes mainly blade wake interaction (BWI) noise and blade self-noise [15]. Broadband frequency region is set from the end of the main BVI region to the end of the spectrum.

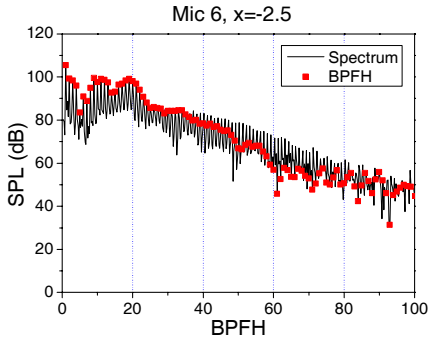

Figure 10: Narrowband spectrum and blade passage frequency harmonics for noise source signal measured at Mic 6 / x=-2.5.

5.2 Signal Re-construction

Consider the spectrum of a noise source signal, as, for example, the one shown in Figure 10. The spectrum can be divided in the frequency regions as discussed above. Firstly, a time signal is created via inverse Fourier transform by considering a constant phase of $-\pi$ for all frequencies up to and excluding the 5th bpfh and zeroing out all other values of the spectrum. A so-constructed signal is shown in Figure 11. By applying the constant phase $-\pi$ in the thickness frequency region, the aim is to create a negatively valued symmetrical pulse that resembles loading/thickness noise.

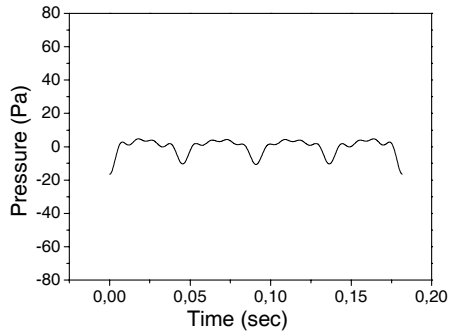

Figure 11: Stage 1 of the phase assignment method: signal corresponding to the thickness frequency region.

Subsequently, a second time signal is created by assigning a constant phase of $-\pi/2$ to all blade passage frequencies and their neighboring shaft frequencies (the quarter bpfh) in the BVI frequency region. To the remaining frequencies in the BVI frequency region, as well as to all frequencies in the broadband noise frequency region, random phases are assigned. The values of the spectrum in the thickness frequency region are zeroed out. A so-constructed signal is shown in Figure 12. Ideally the BVI energy is distributed only to the blade passage harmonics. However, increased unsteadiness and blade-to-blade differences of the acoustic impulses are shown to spread the energy from the blade passage harmonics to the shaft harmonics [14]. Further, the value of the constant phase of $-\pi/2$ is applicable to advancing side BVI signals. For retreating side BVI signals the value of $\pi/2$ is used instead.

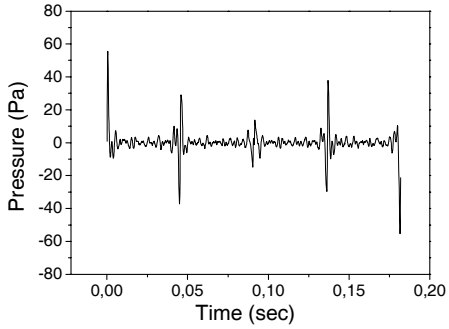

Figure 12: Stage 2 of the phase assignment method: signal corresponding to the main BVI and broadband frequency region.

Finally, the two constructed signals are added together to create the final signal. Before their addition, the signal corresponding to BVI noise (Figure 12) is shifted in time in order to start later than the signal corresponding to the thickness frequency region (Figure 11). The time shift is equal to half the time between the first two blade passages. This is done to simulate the phase difference between thickness and BVI noise. The final signal is shown in Figure 13.

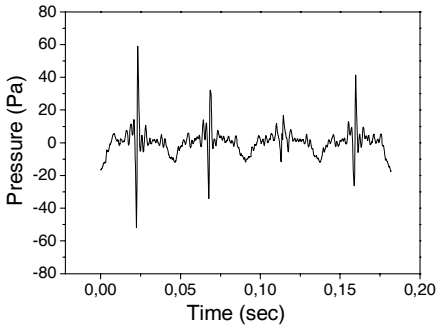

Figure 13: Stage 3 of the phase assignment method: Time shifting of signal under stage 1 and its addition to the time signal under stage 2.

5.3 Prediction Examples

The proposed phase assignment method has been applied to several noise source spectra. Time signals have been constructed from the noise spectra and numerically propagated to predict DSPL. The DSPL yielded from the re-constructed signal through the phase assignment method compares reasonably well with the DSPL yielded from the real noise source signal. The good comparison is shown in

Figure 14 and Figure 15 for receiver locations in both the advancing and retreating BVI side.

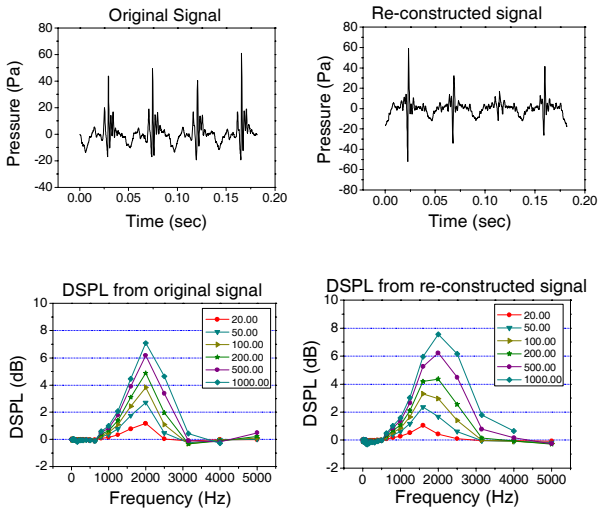

Figure 14: Phase assignment method: Original and re-constructed pressure time signals and their corresponding DSPL plots for various propagation distances; Mic 6 / x=-2.5.

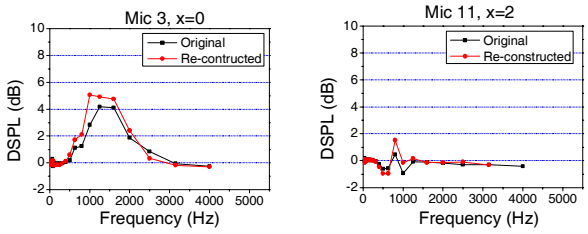

Figure 15: Phase assignment method: Compariosn between DSPL after 1000m of propagation yielded by the original noise source signal and the re-constructed signal; noise source signals at the advancing side Mic 3/ x=0 (l) and the retreating side Mic 11 / x=2 (r).

6 Summary

In summary, nonlinear propagation distortion of helicopter's main rotor noise has been investigated, its effect demonstrated and methods for its prediction presented. Specifically, three methods are presented based on the Burgers Equation: (i) a numerically generated database that provides a rough guideline for DSLP when only the receiver location is known, (ii) correlations between DSPL and various signal characteristics at the source that can be used to determine if a detailed prediction is needed and (iii) a phase-assignment method that allows employment of the Burgers Equation even when the phase information is missing.

Acknowledgments

The work has been partially supported by the European Integrated Project FRIENDCOPTER.

References

[1] S. McInerny, K. L. Gee, M. Dowing, M. James "Acoustical Nonlinearities in Aircraft Flyover Data," *AIAA* Paper 2007-3654 (2007).

[2] H. H. Brouwer, "Numerical Simulation of Nonlinear Jet Noise Propagation," *AIAA* Paper 2005-3088 (2005).

[3] K. L. Gee, V. W. Sparrow, T. B. Gabrielson, A. A. Atchley, "Nonlinear Modeling of F/A-18E Noise Propagation," *AIAA* paper 2005-3089 (2005).

[4] Barger, R. L. Theoretical prediction of nonlinear propagation effects on noise signatures generated by subsonic or supersonic propeller or rotor-blade tips. May 1, 1980. NASA-TP-1660; L-13388.

[5] Nonlinear Acoustics, edited M.F.Hamilton and D.T.Blacktock, Academic press, 1998.

[6] Acoustics: An introduction to its Physical Principles and Applications, Allan D. Pierce, Acoustical Society of America, 1994.

[7] R. O. Cleveland, M. F. Hamilton, D. T. Blackstock, "Time-domain modeling of finite-amplitude sound in relaxing fluids," *J. Acoust. Soc. Am.* 99, 3312-3318 (1996).

[8] Y.-S. Lee, M. F. Hamilton, "Time-domain modeling of pulsed finite-amplitude sound beams," *J. Acoust. Soc. Am.* 97, 906-917 (1995).

[9] Schmitz F.H., Boxwell D.A., Splettstoesser W.R. and Schultz K.J. Model-rotor high speed impulsive noise: Full-scale comparisons and parametric variations, Vertica Vol. 8, No. 4, pp. 395-442, 1984.

[10] K.-J Schultz, W. Splettstoesser, B. Junker, W. Wagner, E. Schoell, E. Mercker, K. Pengel, G. Arnaud, D. Fertis, "A parameteric windtunnel test on rotorcraft aerodynamics and aseroacoustics (Helishape) – test procedures and representative results," 22nd European Rotorcraft Forum, Brighton, UK, 1996.

[11] Schmitz F H: Rotor noise. NASA Ames Research Center, Moffett Field, California, 1991.

[12] P. Menounou and P. Vitsas, "Numerical investigation of the effect of nonlinear propagation distortion on helicopter noise," 155th ASA Meeting and 7th European Conference on Noise Control (Euronoise), Paris, 2008.

[13] Splettstoesser WR, Kube R, Wagner W, Seelhorst U, Boutier A, Micheli F, Mercker E, Pengel K. "Key results from a higher harmonic control aeroacoustic

rotor test (HART).” J American Helicopter Society 1997;42(1).

[14] R. M. Martin. J. C. Hardin, “Spectral Characteristics of Rotor Blade/Vortex Interaction Noise”, J. Aircraft, Vol.25, No. 1, 1987.

[15] T. F. Brooks, M.A. Marcolini, D.S. Pope, “Main Rotor Broadband Noise Study in the DNW”, AHS Specialists’ Meeting on Aerodynamics and Aeroacoustics, Arlington, Texas, 1987.